JMEPEG (2019) 28:4991–4997
https://doi.org/10.1007/s11665-019-04220-x

1059-9495/$19.00

Cyclic Thermal Oxidation Evaluation to Improve Ti6Al4V Surface in Applications as Biomaterial

Carolina Aurélia Ribeiro Maestro, Alysson Helton Santos Bueno, and Artur Mariano de Sousa Malafaia

(Submitted October 12, 2018; in revised form May 30, 2019; published online July 24, 2019)

Thermal oxidation treatments are widely used to modify titanium surfaces. Thermally oxidized titanium alloys are used as biomaterials due to their better surface properties, such as corrosion resistance. However, the use of cyclic thermal treatment for this purpose has not yet been reported. This paper's objective was to compare roughness, microhardness and corrosion resistance after cyclic and conventional isothermal heat treatments in a Ti6Al4V alloy. The heat treatments were performed over a period of 24 h with a maximum temperature of 650 °C, and cyclic conditions were executed from 200 to 400 °C for 48 cycles, each lasting 0.5 h. After the thermal treatments, roughness was measured through profilometer and atomic force microscopy, Vickers microhardness was evaluated, and polarization corrosion tests were performed in simulated body fluid. All treatments increased surface roughness, microhardness and corrosion resistance at 500 mV above open-circuit potential in polarization tests, compared to the material without oxidation. These results are associated with rutile formation, observed through XRD analysis. Although the isothermal and cyclic treatments presented similar behaviors, the 650-200 °C cyclic heat treatment provided an intermediate roughness and produced a slightly better corrosion resistance, demonstrating that cyclic thermal treatments are a viable alternative for improving titanium alloy surface properties.

Keywords biomaterial, corrosion resistance, cyclic heat treatment, roughness, surface modification, thermal oxidation, titanium

1. Introduction

Pure titanium and titanium alloys are noted by their chemical stability, good mechanical properties, biocompatibility, as also corrosion and high temperatures resistance. These characteristics allow for its application in the chemical, aeronautic and biomaterials industries (Ref 1). In regard to biomaterial applications, titanium is used for several different joint replacement prostheses, dental implants and orthodontic surgery parts, bone fixation parts and artificial organs structures, which are used in the orthopedic and dental industries (Ref 2, 3). In most bio-applications, titanium alloys have a wider range of use than pure titanium (CP-Ti), because adding small amounts of alloying elements, such as aluminum and vanadium, increases the strength of the alloy when compared to CP-Ti. Due to its biocompatibility and corrosion resistance, Ti6Al4V is still the $\alpha + \beta$ titanium alloy most often used in biomedical applications, although some current studies contest its long-term use. This concern is due to the possibility of vanadium and aluminum ions being released into the human body, a phenomenon associated with Alzheimer's disease, neuropathy and osteomalacia (Ref 2, 4, 5).

Carolina Aurélia Ribeiro Maestro, Alysson Helton Santos Bueno, and **Artur MarianodeSousa Malafaia**, Universidade Federal de São João Del Rei, Praça Frei Orlando, 170, Centro, São João Del Rei, MG 36307-352, Brazil. Contact e-mail: arturmalafaia@ufsj.edu.br.

For a material to be applied as a biomaterial, several properties are required, including excellent biocompatibility, low density and a low elastic modulus. However, the physicochemical properties of the material's surface are responsible for ensuring cell proliferation and adhesion, osseointegration and for avoiding inflammation and loosening of the implant, which are caused by the release of ions into the body. These physicochemical properties include surface chemistry, hardness and roughness, as well as corrosion resistance in body fluids. Thus, several techniques were developed to alter the surface of pure titanium and titanium alloys for successful implantation (Ref 1, 6), modifying chemically and mechanically the surface, promoting cells proliferation and differentiation (Ref 7), as also bone deposition (Ref 8).

Anodic oxidation, cementation, ion deposition and thermal oxidation are among the different techniques employed to alter titanium surface chemistry. Thermal oxidation treatment is currently one of the most commonly used techniques for modifying titanium alloy surfaces due to its low cost and easy production technique, forming a continuous ceramic film of protective oxide. Several studies have shown that thermal treatments improve the Ti6Al4V surface. These improvements include increased wear resistance (Ref 9), higher microhardness, increased roughness and better corrosion resistance (Ref 10, 11). After evaluating the temperatures of 500, 650 and 800 °C from 8 to 48 h, Kumar et al. (Ref 11) reported that Ti6Al4V has excellent corrosion resistance after using a 650 °C heat treatment for 24 h.

Thermal cycles are normally related to cyclic oxidation tests, which evaluate a material's behavior and resistance for use in high-temperature applications (Ref 12). In comparison with isothermal oxidation tests, the successive cooling steps in thermal cycles promote thermal stresses in the surface that can change the generated roughness and oxide formation and often cause oxide spallation for metals in general (Ref 13), as observed for FeMnSiCrNi alloys (Ref 14, 15) and for Ti-6Al-

2Sn-4Zr-2Mo (Ref 16). The use of thermal cyclic variation during heat treatments in metals is mainly reported with regard to the formation of spheroidite in carbon steels (Ref 17). In titanium alloys, cyclic heat treatments are used to promote modification to microstructure and mechanical properties (Ref 16, 18, 19), but the use of cyclic heat treatments with the aim of improving surface characteristics of titanium and titanium alloys have not previously been reported.

Considering that cyclic thermal treatments, when compared to isothermal treatments, can generate different modifications to the oxide scale formed on the surface of a titanium alloy, the aim of the present study was to evaluate the use of cyclic heat treatments in a Ti6Al4V alloy to promote better properties related to its use as a biomaterial. For this evaluation, the samples' roughness, microhardness and corrosion resistance were accessed after performing different heat treatments.

2. Materials and Methods

2.1 Sample Preparation

Ti-6Al-4V disk samples with a thickness of approximately 5 mm were cut from a 17.25 mm diameter bar. The procedure was executed slowly and coolant fluid was used to avoid any microstructure change by heating. The two sides of the sample were sanded using SiC papers (#80, 120, 240, 360, 500, 600, 800, 1000, 1500 and 2000), followed by mirror polishing with 1 μm alumina suspension. They were then cleaned in an ultrasound bath using isopropyl alcohol, acetone and then distilled water (30 min in each liquid). The samples were dried using hot air and, just before oxidation tests, a pickling step was performed to remove any impurities and the passive oxide layer (TiO_2), as previously reported (Ref 20). The samples were immersed for approximately 60 s in the pickling solution, which was composed of 35 vol.% HNO_3 and 5 vol.% HF in distilled water, heated to 40 °C, followed by an immersion into distilled water and hot air drying. With respect to microstructure characterization, one sample was chemically pickled after polishing using Kroll's reagent (100 ml H_2O, 5 ml HNO_3 and 3 ml HF) and observed through scanning electron microscope (SEM).

2.2 Sample Oxidation

Three different surface heat treatments were performed, one isothermal and two cyclic. The furnace used allowed for Z-axis movement, exhibiting up and down positions, in which the samples are either inside or outside of the furnace, respectively. For all tests, the maximum temperature was set at 650 °C and the furnace was heated to this maximum temperature in the down position before moving to the up position. Thus, during the entire procedure, the furnace was maintained at maximum temperature and the samples were exposed to this temperature when it was in the high position. The furnace was equipped with two k-type thermocouples, one close to the kanthal resistance wires, determining the furnace temperature and the second one inside a quartz tube close to the samples, determining their temperatures. The isothermal oxidation treatments were carried out during a period of 24 h, followed by cooling inside the furnace in order to avoid high thermal stresses. The cyclic oxidation treatments were performed between the temperatures of 650 and 400 °C or 650 and 200 °C, in 48 cycles of 30 min, i.e., after achieving the maximum temperature, the furnace moved up to the first cycle, stayed there for 30 min and automatically moved to the down position until the sample temperature reached 400 or 200 °C, respectively, at which point the furnace moved to the up position again and started a new cycle. Therefore, the cyclic samples were exposed to 650 °C for a period of 24 h, the same amount of time as the isothermal tests. The final cooling was performed inside the furnace, similar to the isothermal treatment. Inside the apparatus, the samples were hung by a hole using a wire, which allowed the surface to be completely exposed to the furnace's atmosphere (laboratory air). After the thermal treatments, the formed oxide layer was characterized by x-ray diffraction (XRD) using Cu-Kα radiation and 2θ-angle scanning from 10° to 80°, as also topographically by SEM. The nomenclatures used for the heat treatments in the present article are as follows: isothermal, cyclic 650-400 and cyclic 650-200.

2.3 Microhardness and Roughness Measurements

Vickers microhardness was determined in two different samples of each condition, untreated (polished) and heat-treated, using a load of 0.2 kg for 20 s. For the polished sample, five measurements were taken. For the oxidized samples, due to some scattered results, eleven measurements were taken and the two highest and two lowest were discarded. For all conditions, the average and standard deviation were calculated.

The *Ra* and *Rz* roughnesses were also evaluated for the polished sample surfaces and then evaluated again after thermal treatments. The measurements were taken using 80 μm cutoff and 5 mm length. For all samples, two of each condition, five measurements were taken to determine the average. The oxidized samples were also observed through atomic force microscopy (AFM), determining *Ra* and *Rm*s roughnesses in areas from 74 to 91 μm^2 at a probe speed of 0.64 to 0.92 Hz.

2.4 Potentiodynamic Polarization Tests

Polarization electrochemical tests were performed in an Autolab Multi Potentiostat model PGSTAT101, using a flat cell, platinum counter electrode, saturated calomel reference electrode and simulated body fluid (SBF) solution. The SBF was prepared following the instructions published by Kokubo (Ref 21), and Table 1 shows the component ratios, as well the sequence in which each component was added. Untreated

Table 1 Component amounts and sequence of additions to prepare 1000 ml of simulated body fluid (SBF). Adapted from [21]

Order	Reagent	Amount
1	NaCl	8.035 g
2	$NaHCO_3$	0.355 g
3	KCl	0.225 g
4	$K_2HPO_4 \cdot 3H_2O$	0.231 g
5	$MgCl_2 \cdot 6H_2O$	0.311 g
6	1.0 $_M$-HCl	39 ml
7	$CaCl_2$	0.292 g
8	Na_2SO_4	0.072 g
9	Tris	6.118 g
10	1.0 $_M$-HCl	0-5 ml

(polished), isothermal treated and cyclic treated samples were evaluated. During the tests, the sample was exposed to the solution by means of a hole on the side of the corrosion flat cell, containing a rubber O-ring. The area of the hole was around 1 cm^2, and to avoid the use of welding, since titanium is not easily welded, bevels were put into the sample borders to plug the potentiostat cables directly on the sample. The SBF solution was maintained at 39 °C to simulate an extreme human body temperature situation. Before the polarization tests, the OCP was determined, followed by a scan from OCP to 2 V above it at a rate of 0.5 mV/s. The OCP value was determined after 1 h of sample's contact with the solution, by continuous potential measurement, allowing stabilization. The tests were carried out two times in each condition, and the results presented here are an average of both tests. To compare different tests and determine the best results as a basis for criteria, Kumar et al. (Ref 11) considered the value in the passive region to be i_{pass} at 1000 mV. In the current study, the values of E_{corr} and current density at 500 mV above OCP (I_{500mV} in the passivation region) were determined from two polarization curves for each condition. After corrosion tests, the oxidized samples were observed by SEM to evaluate the presence of pits on the surface.

3. Results and Discussion

3.1 Microstructure and Oxide Layer Characterization

The Ti6Al4V alloy is the biocompatible alloy most employed in orthopedic and orthodontic prosthesis (Ref 11, 22). Figure 1(a) presents the microstructure after metallographic preparation and before oxidation tests. The alpha phase is present as the base material and the beta phase in dark lamellas, which compose the alpha + beta microstructure. The EDS analysis, shown in the upper right side of Fig. 1, determines the alloy chemical composition. Although the amount of aluminum was within the recommended range of ASTM F136, the amount of vanadium was below the minimum, suggesting that the alloy's composition was slightly off.

Figure 1(b), (c), (d) and (e) reveals the topographic view of oxide layer formed after isothermal and cyclic oxidation. The morphological aspect was the same for the three heat treatments, and thus, the pictures presented here were related only to isothermal (Fig. 1b and d) and cyclic 650-200 (Fig. 1c and e). At low magnification (Fig. 1b and c) was possible to notice the alpha–beta microstructure details, revealing a thin oxide layer. Higher magnification (Fig. 1d and e) allowed observing a similar granulometry after the different heat treatments.

Figure 2 presents the x-ray diffraction data for untreated material and also after the three different heat treatments. For the base material (untreated sample), the Ti-alpha hexagonal phase was determined. The substrate was also observed after all heat treatments, but showing higher peaks of rutile (TiO_2), evidencing its formation as also some small peaks related to anatase oxide after cyclic oxidation. The data from the isothermally oxidized sample presented high noise, making it difficult to identify anatase, an oxide detected in small peaks within the cyclically oxidized samples. Fargas et al. (Ref 16) reported the presence of anatase and rutile in a Ti-6Al-2Sn-4Zr-2Mo alloy after cyclic oxidation tests, but after isothermal oxidation, only the presence of rutile was observed. For all samples tested in the current study, the presence of small peaks of metallic titanium (substrate) establishes that the formed rutile layer was thin, due to the fact that no spalled areas were observed. Kumar et al. (Ref 11), while studying the same alloy and using the same isothermal oxidation procedure (650 °C—24 h), also observed rutile formation, in addition to some small substrate peaks. Among different titanium oxides, rutile is favoured since it increases hardness and improves resistance to corrosion and wear (Ref 9, 11, 23).

Figure 3 displays the microhardness determined in untreated and oxidized samples. The hardness after isothermal treatment was twice as high as in untreated samples and the samples after cyclic thermal treatments presented values slightly smaller than the isothermal ones. When considering the error bars, it is possible to consider that all the treatments had similar behavior

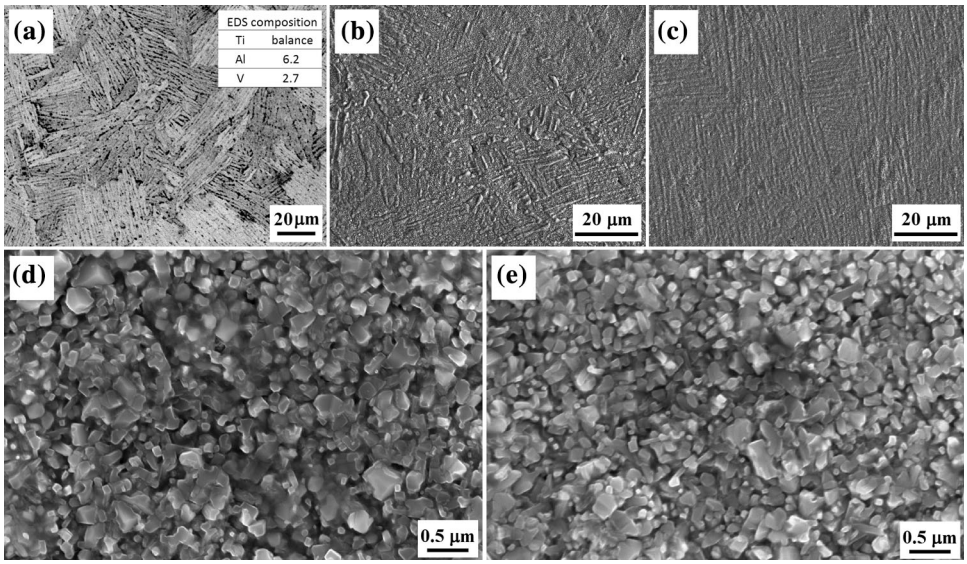

Fig. 1 SEM characterization in the base material and treated samples: (a) alloy microstructure and EDS analysis and (b–e) topographic view after isothermal (b and d) and 650-200 cyclic heat treatment (c and e)

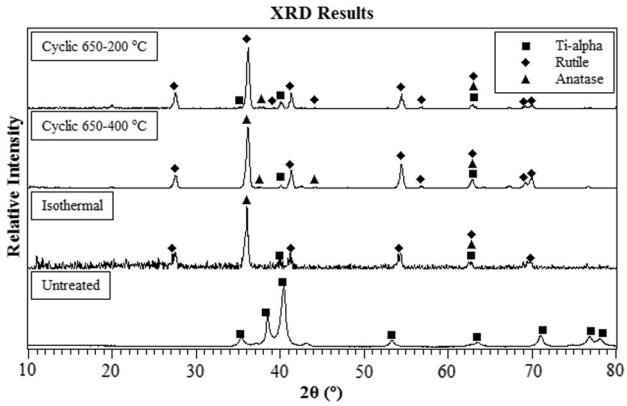

Fig. 2 XRD diffraction of sample surfaces after cyclic and isothermal heat treatments and also untreated material

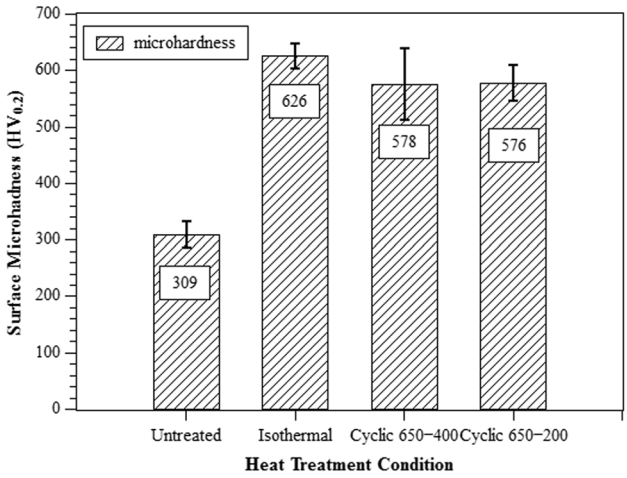

Fig. 3 Surface microhardness determined for untreated, cyclic and isothermally heat-treated samples

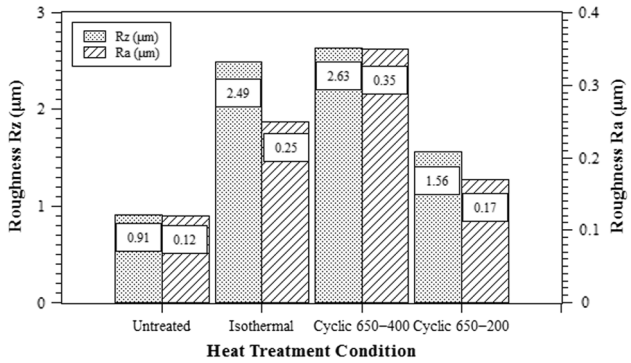

Fig. 4 *Rz* and *Ra* surface roughness measurements for untreated and heat-treated samples

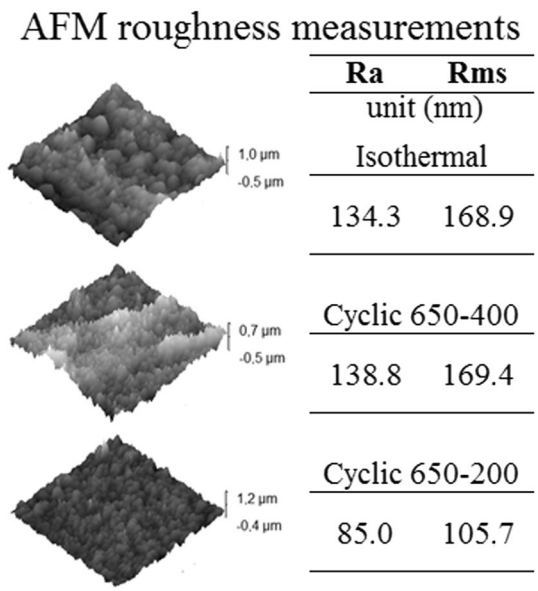

Fig. 5 AFM roughness measurements for heat-treated sample surfaces

and increased superficial microhardness, which is considered to be an important characteristic in bio-applications, seeing that this property can help to avoid wear (Ref 9, 23). The hardness value of 309 ± 23 $HV_{0.2}$ observed here for the untreated sample was close to the value observed by Kumar et al. (Ref 11), 324 ± 8, for the same alloy. Contrarily, they observed a value higher than 800 $HV_{0.2}$ for the same isothermal treatment performed in this study, in which a value of 626 ± 22 $HV_{0.2}$ was achieved. Values in this range were observed by Kumar et al. (Ref 11) after oxidation for only 8 h at the same temperature.

Another important characteristic regarding the use of Ti alloys in bio-applications is surface roughness. *Ra* and *Rz* values for all conditions are shown in Fig. 4, and AFM *Ra* and *Rm*s measurements are presented in Fig. 5 for only the heat-treated samples. Increased roughness was observed for all heat-treated samples, as also presented in previous studies (Ref 11, 23). The values observed for untreated samples are close to those observed by Kumar et al. (Ref 11). For the isothermal samples, the values are smaller than those observed by Kumar et al. (Ref 11) in the same conditions. The cyclic oxidized samples presented different behaviors; the 650-400 sample presented the highest *Ra* and *Rz* values, while the 650-200 sample presented the smallest values in relation to the heat-treated samples. The same behavior was observed in the AFM measurements (Fig. 5), showing that the 650-400 cyclic treatment tends to promote a slightly higher roughness compared to the isothermal treatment, whereas the 650-200 cyclic treatment generates a substantially smaller roughness. Kim et al. (Ref 24) determined that a smooth surface (*Ra* = 0.18) promotes better osteoblast cell proliferation than a rougher surface (*Ra* = 2.95). Regarding *Rz*, Ponsonnet et al. (Ref 25) observed better fibroblast cell proliferation for *Rz* values below 1.0. Taking into consideration the results presented in this study, the sample oxidized by the 650-200 heat treatment presented better *Ra* and *Rz* values compared to the above-mentioned articles, although there is no congruence related to the best roughness value for better biocompatibility. For example, Zhu et al. (Ref 26) studied two different electrolytes to evaluate osteoblast cell attachment and determined that better attachment for one electrolyte was achieved by decreasing roughness and for the other electrolyte, increasing roughness achieved better attachment (studying samples between $0.1 \leq Ra \leq 0.5$).

The increase in roughness during thermal oxidation can be related to the oxide growth stress (present in both isothermal and cyclic oxidation) and also generated by the coefficient of thermal expansion (CTE) mismatch between the oxide and substrate (only present during the cooling steps in cyclic oxidation) (Ref 13, 27, 28). Considering that the highest thermal variation and the smallest roughness generated among heat-treated samples were observed in the 650-200 sample, the CTE mismatch between rutile and substrate seems to not have contributed to the increase in roughness. The CTEs of rutile (8.2×10^{-6}) (Ref 29) and Ti6Al4V (10.0×10^{-6}) (Ref 28) do not greatly differ. In cyclic oxidation tests with maximum temperatures of 550, 650, 750 or 850 °C, followed by 10 min of cooling, Zeng et al. (Ref 28) observed cracks and spallation only for samples oxidized at 750 and 850 °C. This result demonstrates that cyclic oxidation at 650 °C does not generate high stress and it is important to consider here that the minimum temperature was 200 °C, which avoided a high temperature variation. The oxide growth stress is related to the Pilling–Bedworth ratio; it is compressive to values higher than 1, and the value for rutile is 1.73 (Ref 13). The present results suggest that the oxide growth stress promotes the increase in roughness and that cyclic intervals between 650 and 200 interrupt increasing compressive stress, which in turn develop a low roughness. As the cycles between 650 and 400 are faster and maintain the sample in oxidizing temperatures for more time, the same mechanism does not take place. In the AFM images (Fig. 5), a flatter surface in the 650-200 sample can be observed, which corroborates with the presented discussion.

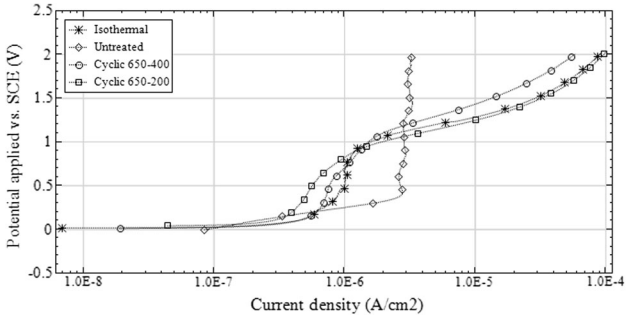

Fig. 6 Curves obtained for untreated and heat-treated samples in polarization tests using SBF solution

Table 2 Corrosion tests data: average and standard deviation values of polarization tests: open-circuit potential and density current 500 mV above OCP (I_{500mV})

Heat treatment condition	OCP, mV	I_{500mV}, A/cm^2
Untreated	32.5 ± 40.5	$(2.8 \pm 0.1) \times 10^{-06}$
Isothermal	8.0 ± 4.0	$(7.7 \pm 2.2) \times 10^{-07}$
Cyclic 650-400	7.5 ± 2.5	$(8.6 \pm 0.9) \times 10^{-07}$
Cyclic 650-200	21.5 ± 15.5	$(5.85 \pm 0.05) \times 10^{-07}$

3.2 Polarization Tests

The corrosion resistance of samples thermally oxidized was evaluated using SBF in polarization tests. The polarization curves in Fig. 6 demonstrate that below 1000 mV, all the samples presented a passive region, which establishes that the oxide layer was protecting the material. After approximately 1000 mV, the current's density started to increase for the heat-treated samples, suggesting pit corrosion. When comparing the three treatments, the behaviors were very similar and had almost the same resistance to corrosion. The samples without heat treatment presented a higher passive region, although the current's density was higher, which affirms that the heat treatments improve corrosion resistance in potentials lower than 1000 mV. On the other hand, the untreated samples maintained the passive film for higher potentials. This occurred because the passive film formed in the untreated sample surfaces during the polarization tests presented less defects than the oxide layer developed in the high temperature. Based on these results and considering that there are no conditions in clinical reality where high potentials are applied (Ref 11), the presently studied heat treatments clearly represent an improvement in corrosion resistance, similar to what other authors have observed for isothermal heat treatments (Ref 9, 11, 23).

The values of OCP and current density measured 500 mV above OCP are presented in Table 2 (including standard deviation). The smallest average values of I_{500mV} were obtained for the samples oxidized cyclically between 650 and 200 °C ($5.85 \pm 0.05 \times 10^{-7}$ A/cm^2). When comparing untreated to heat-treated samples, the latter presented better results of I_{500mV}

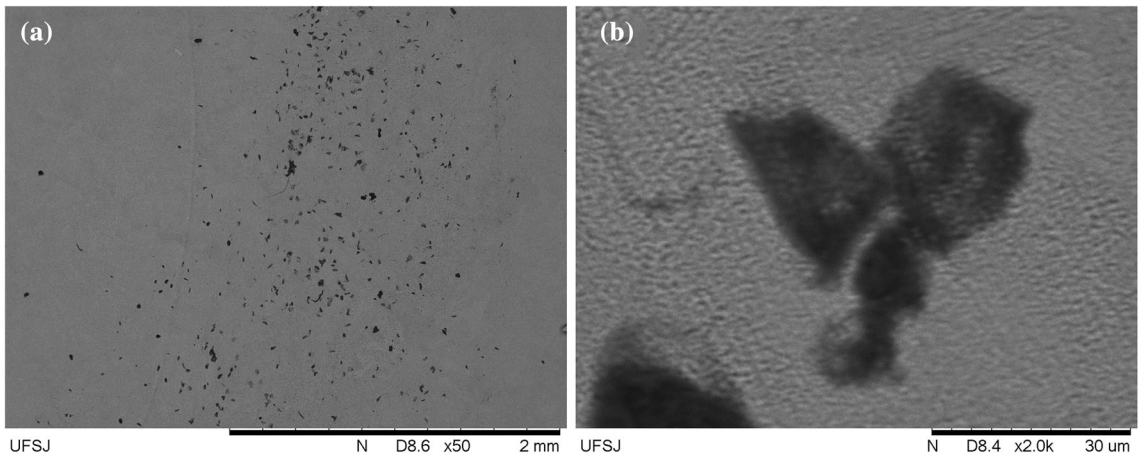

Fig. 7 650-200 sample characterization after polarization tests: (a) pits observed near the sample border and (b) pitting details

in all cases, with values between $5.85 \pm 0.05 \times 10^{-7}$ and $8.6 \pm 0.9 \times 10^{-7}$ A/cm^2 for thermal oxidized samples, against $2.8 \pm 0.1 \times 10^{-6}$ A/cm^2 for untreated sample. These results were already expected for the isothermally oxidized sample, based on previous studies as the rutile-rich oxide layer formed during heat treatments protects the material against corrosion (Ref 11, 23). Furthermore, the present results demonstrate that cyclic oxidized samples also achieve better properties than an untreated sample, with emphasis on the 650-200 condition.

3.2.1 Sample Characterization after Polarization Tests. The polarization curves suggest pit formation in the heat-treated samples. Figure 7 presents the 650-200 sample's surface after the polarization test. The pits observed in Fig. 7(a) were found in the borders of the sample, and Fig. 7(b) presents one of those pits in detail. After polarization tests, these pit formations were also found in SEM observations in the same regions of the sample surfaces of isothermal and cyclic 650-400 oxidized. As shown in the methodology, the sample was outside of the test cell and one side was exposed to the chemical solution. The pits observed in the samples were found near the region where the sample touched the O-ring, forming a circular region with several pits. The occurrence of pits in these regions suggests corrosion by differential aeration (Ref 30). This phenomenon also explains the behavior of the polarization curves, in which the current increased above 1 V potential. Kumar et al. (Ref 11) also used a corrosion flat cell, which presented similar polarization curves to samples oxidized at 500 °C, although no comments regarding the behavior were presented. As mentioned before, there is no case in clinical reality that can promote 1 V potential in implants; thus, no attempts were made to avoid this differential aeration during testing.

4. Conclusions

The isothermal (650 °C—24 h) and cyclic (650-400 and 650-200 °C—48 cycles) heat treatments were performed on a Ti6Al4V alloy as also untreated Ti6Al4V samples for comparison. The heat-treated samples achieved higher hardness and roughness, in addition to better corrosion resistance when compared to the untreated sample, based on I_{500mV}, behavior which is related to the rutile formation on the surface. When comparing the three different treatments, similar results were observed in all tests. However, even though it is not clear if cyclic oxidation can provide improvements in applications using Ti6Al4V, the 650-200 cyclic sample presented the smallest amount of roughness, explained by a proposed mechanism. Regarding corrosion tests, considering the parameter I_{500mV}, the 650-200 sample presented a slightly better corrosion resistance than the isothermal sample (5.85×10^{-7} vs. 7.7×10^{-7} A/cm^2), which suggest that further studies in cyclic oxidation treatments to improve surface preparation for Ti6Al4V as a biomaterial should be performed.

Acknowledgments

The authors would like to acknowledge FAPEMIG—Minas Gerais State Agency for Research and Development for the undergraduate research scholarship. We are also grateful to Prof. Dr. Lecino Caldeira for XRD measurements, Prof. Dr. Thalita Chiaramonte for AFM measurements and CMTC—Grenoble INP for SEM characterizations and also XRD tests.

References

1. M.T. Mohammed, Z.A. Khan, and A.N. Siddiquee, Beta Titanium Alloys: The Lowest Elastic Modulus for Biomedical Applications: A Review, *Int. J. Chem. Mol. Nucl. Mater. Metall. Eng.*, 2014, **8**, p 821–827. https://doi.org/10.5281/zenodo.1094481
2. M. Geetha, A.K. Singh, R. Asokamani, and A.K. Gogia, Ti Based Biomaterials, the Ultimate Choice for Orthopaedic Implants—A Review, *Prog. Mater Sci.*, 2009, **54**, p 397–425. https://doi.org/10.1016/j.pmatsci.2008.06.004
3. M. Niinomi, Recent Research and Development in Titanium Alloys for Biomedical Applications and Healthcare Goods, *Sci. Technol. Adv. Mater.*, 2003, **4**, p 445–454. https://doi.org/10.1016/j.stam.2003.09.002
4. S. Nag, R. Banerjee, and H.L. Fraser, Microstructural Evolution and Strengthening Mechanisms in Ti-Nb-Zr-Ta, Ti-Mo-Zr-Fe and Ti-15Mo Biocompatible Alloys, *Mater. Sci. Eng. C*, 2005, **25**, p 357–362. https://doi.org/10.1016/j.msec.2004.12.013
5. E. Eisenbarth, D. Velten, M. Müller, R. Thull, and J. Breme, Biocompatibility of β-Stabilizing Elements of Titanium Alloys, *Biomaterials*, 2004, **25**, p 5705–5713. https://doi.org/10.1016/j.biomaterials.2004.01.021
6. B.D. Boyan, T.W. Hummert, D.D. Dean, and Z. Schwartz, Role of Material Surfaces in Regulating Bone and Cartilage Cell Response, *Biomaterials*, 1996, **17**, p 137–146. https://doi.org/10.1016/0142-9612(96)85758-9
7. Z. Schwartz, J.Y. Martin, D.D. Dean, J. Simpson, D.L. Cochran, and B.D. Boyan, Effect of Titanium Surface Roughness on Chondrocyte Proliferation, Matrix Production, and Differentiation Depends on the State of Cell Maturation, *J. Biomed. Mater. Res.*, 1996, **30**, p 145–155. https://doi.org/10.1002/(SICI)1097-4636(199602)30:2<145::AID-JBM3>3.0.CO;2-R
8. B. Chehroudi, D. McDonnell, and D.M. Brunette, The Effects of Micromachined Surfaces on Formation of Bonelike Tissue on Subcutaneous Implants as Assessed by Radiography and Computer Image Processing, *J. Biomed. Mater. Res.*, 1998, **34**, p 279–290. https://doi.org/10.1002/(SICI)1097-4636(19970305)34:3<279::AID-JBM2>3.0.CO;2-H
9. F. Borgioli, E. Galvanetto, F. Iozzelli, and G. Pradelli, Improvement of Wear Resistance of Ti-6Al-4V Alloy by Means of Thermal Oxidation, *Mater. Lett.*, 2005, **59**, p 2159–2162. https://doi.org/10.1016/j.matlet.2005.02.054
10. A. Gutiérrez, F. Pászti, A. Climent-Font, J.A. Jiménez, and M.F. López, Comparative Study of the Oxide Scale Thermally Grown on Titanium Alloys by Ion Beam Analysis Techniques and Scanning Electron Microscopy, *J. Mater. Res.*, 2008, **23**, p 2245–2253. https://doi.org/10.1557/JMR.2008.0281
11. S. Kumar, T.S.N. Sankara Narayanan, S. Ganesh Sundara Raman, and S.K. Seshadri, Thermal Oxidation of Ti6Al4V Alloy: Microstructural and Electrochemical Characterization, *Mater. Chem. Phys.*, 2010, **119**, p 337–346. https://doi.org/10.1016/j.matchemphys.2009.09.007
12. J.R. Nicholls and M.J. Bennett, Cyclic Oxidation—Guidelines for Test Standardisation, Aimed at the Assessment of Service Behaviour†, *Mater. High Temp.*, 2000, **17**, p 413–428. https://doi.org/10.1179/mht.2000.17.3.005
13. H.E. Evans, Stress Effects in High Temperature Oxidation of Metals, *Int. Mater. Rev.*, 1995, **40**, p 1–40. https://doi.org/10.1179/imr.1995.40.1.1
14. A.M. De Sousa Malafaia, V.R. do Nascimento, L. Mendes Sousa, M. Eduardo, and M.F. de Oliveira, Anomalous Cyclic Oxidation Behaviour of an Fe-Mn-Si-Cr-Ni Alloy—A Finite Element Analysis, *Corros. Sci.*, 2019, **147**, p 223–230. https://doi.org/10.1016/j.corsci.2018.11.018
15. A.M. de Sousa Malafaia and M.F. De Oliveira, Anomalous Cyclic Oxidation Behaviour of a Fe-Mn-Si-Cr-Ni Shape Memory Alloy, *Corros. Sci.*, 2017, **119**, p 112–117. https://doi.org/10.1016/j.corsci.2017.02.026
16. G. Fargas, J.J. Roa, B. Sefer, R. Pederson, M.L. Antti, and A. Mateo, Influence of Cyclic Thermal Treatments on the Oxidation Behavior of Ti-6Al-2Sn-4Zr-2Mo Alloy, *Mater. Charact.*, 2018, **145**, p 218–224. https://doi.org/10.1016/j.matchar.2018.08.049

17. C.C. Chou, P.W. Kao, and G.H. Cheng, Accelerated Spheroidization of Hypoeutectoid Steel by the Decomposition of Supercooled Austenite, *J. Mater. Sci.*, 1986, **21**, p 3339–3344. https://doi.org/10.1007/BF00553377
18. W. Szkliniarz, J. Chrapoński, A. Kościelna, and B. Serek, Substructure of Titanium Alloys After Cyclic Heat Treatment, *Mater. Chem. Phys.*, 2003, **81**, p 538–541. https://doi.org/10.1016/S0254-0584(03)00069-5
19. Z. Lv, X. Ren, Z. Li, Z. Lu, M. Gao, and T. Beijing, Effects of Two Different Cyclic Heat Treatments on Microstructure and Mechanical Properties of Ti-V Microalloyed Steel, *Mater. Res.*, 2015, **18**, p 304–312. https://doi.org/10.1590/1516-1439.302414
20. S. Izman, M. Rafiq, M. Anwar, E.M. Nazim, R. Rosliza, A. Shah, M.A. Hass, Surface Modification Techniques for Biomedical Grade of Titanium Alloys: Oxidation, Carburization and Ion Implantation Processes, in: Titanium Alloys-Towards Achieving Enhanced Properties for Diversified Applications (InTech, 2012), pp. 201–228. https://doi.org/10.5772/36318
21. T. Kokubo and H. Takadama, How Useful is SBF in Predicting in Vivo Bone Bioactivity?, *Biomaterials*, 2006, **27**, p 2907–2915. https://doi.org/10.1016/J.BIOMATERIALS.2006.01.017
22. C.N. Elias, Y. Oshida, J.H.C. Lima, and C.A. Muller, Relationship Between Surface Properties (Roughness, Wettability and Morphology) of Titanium and Dental Implant Removal Torque, *J. Mech. Behav. Biomed. Mater.*, 2008, **1**, p 234–242. https://doi.org/10.1016/j.jmbbm.2007.12.002
23. A. Bloyce, P. Qi, H. Dong, and T. Bell, Surface Modification of Titanium Alloys for Combined Improvements in Corrosion and Wear Resistance, *Surf. Coat. Technol.*, 1998, **107**, p 125–132. https://doi.org/10.1016/S0257-8972(98)00580-5
24. H.J. Kim, S.H. Kim, M.S. Kim, E.J. Lee, H.G. Oh, W.M. Oh, S.W. Park, W.J. Kim, G.J. Lee, N.G. Choi, J.T. Koh, D.B. Dinh, R.R. Hardin, K. Johnson, V.L. Sylvia, J.P. Schmitz, and D.D. Dean, Varying Ti-6Al-4V Surface Roughness Induces Different Early Morphologic and Molecular Responses in MG63 Osteoblast-Like Cells, *J. Biomed. Mater. Res. Part A*, 2005, **74A**, p 366–373. https://doi.org/10.1002/jbm.a.30327
25. L. Ponsonnet, K. Reybier, N. Jaffrezic, V. Comte, C. Lagneau, M. Lissac, and C. Martelet, Relationship Between Surface Properties (Roughness, Wettability) of Titanium and Titanium Alloys and Cell Behaviour, *Mater. Sci. Eng. C*, 2003, **23**, p 551–560. https://doi.org/10.1016/S0928-4931(03)00033-X
26. X. Zhu, J. Chen, L. Scheideler, R. Reichl, and J. Geis-Gerstorfer, Effects of Topography and Composition of Titanium Surface Oxides on Osteoblast Responses, *Biomaterials*, 2004, **25**, p 4087–4103. https://doi.org/10.1016/j.biomaterials.2003.11.011
27. A.M. Huntz, Stresses in NiO, Cr2O3 and Al2O3 Oxide Scales, *Mater. Sci. Eng. A*, 1995, **201**, p 211–228. https://doi.org/10.1016/0921-5093(94)09747-X
28. S. Zeng, A. Zhao, H. Jiang, X. Fan, X. Duan, and X. Yan, Cyclic Oxidation Behavior of the Ti-6Al-4V Alloy, *Oxid. Met.*, 2014, **81**, p 467–476. https://doi.org/10.1007/s11085-013-9458-z
29. S.S. Jiang and K.F. Zhang, Study on Controlling Thermal Expansion Coefficient of ZrO_2-TiO_2 Ceramic Die for Superplastic Blow-Forming High Accuracy Ti-6Al-4V Component, *Mater. Des.*, 2009, **30**, p 3904–3907. https://doi.org/10.1016/J.MATDES.2009.03.023
30. A.J. Spark, I. Cole, D. Law, D. Marney, and L. Ward, Investigation of Agar as a Soil Analogue for Corrosion Studies, *Mater. Corros.*, 2016, **67**, p 7–12. https://doi.org/10.1002/maco.201508312